Mechanics Research Communications 90 (2018) 18–25

Contents lists available at ScienceDirect

Mechanics Research Communications

journal homepage: www.elsevier.com/locate/mechrescom

Numerical simulation of a water droplet splash: Effects of density interpolation schemes

Douglas Hector Fontes[a,*], Carlos Antonio Ribeiro Duarte[b], Francisco José de Souza[a]

[a] School of Mechanical Engineering, Federal University of Uberlândia, João Naves de Ávila Avenue, 2121, bloco 5P, Uberlândia 38400-902, Minas Gerais, Brazil
[b] Department of Engineering, Federal University of Goiás - Regional Catalão, Dr. Lamartine Pinto de Avelar, Catalão, Goiás 1120, Brazil

ARTICLE INFO

Article history:
Received 7 March 2018
Revised 23 March 2018
Accepted 6 April 2018
Available online 7 April 2018

Keywords:
VoF schemes
Unstructured mesh
Splash
Droplet

ABSTRACT

Flows of two immiscible fluids are widely found in many industrial and natural applications, such as: refrigeration, combustion, irrigation, rain and cavitation. The comprehension/prediction of these kind of flows, simply termed henceforward as two-phase flows, is very important. In this work, water droplet splash cases were studied numerically. This problem is a very interesting two-phase flow, since it occurs in film formation problems, and reliable experimental measures are easily obtained (which is rare in two-phase flow problems), being found in the literature. The VoF model was employed to simulate the impact of a water droplet on a water pool. Although the geometrical schemes, such as PLIC (Piecewise-Linear Interface Calculation) has been demonstrated to yield good results for this problem, it is a rather complex, computationally expensive method, especially when applied to unstructured meshes in many practical problems. Instead, the CICSAM scheme (Compressive Interface Capturing Scheme for Arbitrary Meshes) was used in this work because of its low computational cost and accuracy. The effect of four different schemes for the density interpolation was investigated: central difference, first-order upwind, the second-order and volume fraction weighted. All simulations were compared with experimental data for both the crater depth and ascending jet resulting from the droplet impact. In general, good agreement for the crater depth was found for all the density interpolation schemes, although the volume fraction weighted scheme produced the best results for the ascending jet height. Thus, the VoF/CICSAM method, mainly using the volume fraction weighted scheme for density, proved to be computationally cheaper and reliable to analyze the water droplet splash cases. The methodology presented in this work can be extended to other two-phase flows applications.

1. Introduction

Two-phase flows are frequently encountered in numerous practical problems, such as fuel injection, irrigation, free surface flows and jet painting [19,20,27,29]. The comprehension and ability to predict the interaction between liquid and gas phases are crucial to improve the control over a variety of systems. Numerical modeling has shown some advantages over experiments, especially in the study of two-phase flows by allowing feasible analysis on regions impossible to access (e.g., high temperature, high pressure and primary liquid breakup) [1,6,21]; and complete visualization of the flow fields (e.g., velocity, interface and temperature) without intrusive probes. Proper numerical evaluation and transportation of the interface between gas and liquid phases can be handled through different approaches. Among them, the most employed are the Front-Tracking [31], Level Set [30] and the VoF (Volume of Fluid) [32] methods. The VoF method is locally and globally mass conserving [10], thus being an attractive option for two-phase flow simulations.

Numerical validation has become a major concern in many practical applications. Basically, the procedure consists in simulating a problem for which experiments or an exact solution exists, and comparing them with the simulation results to verify the consistency and features of the implemented methods. Although there are several well-documented experiments on gas-liquid flows [4,16,26],the impact of a water drop onto a deep water pool, simply water droplet splash, is an interesting case for testing numerical schemes, since experimental visualization is relatively easy and reliable. Despite the water droplet splash can be thought as a simple problem, it represents a building block for the investigation of liquid films, for example. The water droplet splash problem is basically a water drop that impacts on the surface of the water pool. This impact creates a crater that reaches a maximum depth. The

* Corresponding author.
E-mail address: douglas.fontes@ufu.br (D.H. Fontes).

https://doi.org/10.1016/j.mechrescom.2018.04.003
0093-6413/

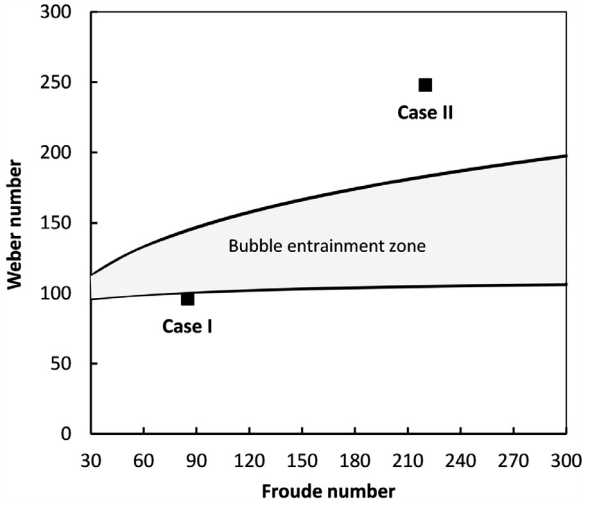

Fig. 1. Map showing the bubble entrainment zone for different conditions based on the Weber and Froude numbers, adapted from [24].

combination of surface tension and gravitational effects leads the gas-liquid interface to an hydrostatic condition. From crater formation to hydrostatic condition, the impact of the water drop on the pool can generate bubble entrainment, ascending liquid jet and other coherent structures. Consequently, the temporal evolution of this problem is highly dependent on the surface tension, inertial effects and gravitational field. In dimensional analysis terms, these phenomena can be represented by two important dimensionless parameters, namely the Weber and Froude numbers. The former expresses the ratio between the inertial forces and the surface tension forces, while the latter is the ratio of the inertial forces on an element of fluid to the weight of the fluid element. They are given by the following equations, Eqs. (1) and (2),

$$We = \frac{\rho_l U_l^2 D}{\sigma}, \tag{1}$$

$$Fr = \frac{U_l^2}{gD}, \tag{2}$$

where ρ_l is liquid density, σ is the interfacial tension between liquid and gas phases, U_l is the impact drop velocity, and D is drop diameter. Oguz and Prosperetti [24] mapped the bubble entrainment zone using experimental data from Pumphrey and Crum [25]. These authors identified bubble entrainment for some physical conditions of the drop impact and related them to the Weber and Froude numbers. As a result, they concluded that the bubble entrainment is contained by two curves, as shown in Fig. 1. In Fig. 1, the solid lines are the least-square fit of the experimental data of Pumphrey and Crum [25] with the form of $We = AFr^B$. The upper line gives $A = 48.3$ and $B = 0.247$ while the lower line $A = 41.3$ and $B = 0.179$.

Morton et al. [23] and Hernández et al. [17] performed numerical validations considering two conditions of a water drop impacting a deep water pool. Both cases were characterized by the following dimensionless numbers: *Case I* - $We = 96$ and $Fr = 85$; *Case II* - $We = 248$ and $Fr = 220$ and were marked in Fig. 1. From the graph, it can be concluded that only in *Case I* bubble entrainment is expected to occur. The numerical solution employed by Morton et al. [23] consisted of discretizing both momentum and continuity equations using the finite-difference method [14] on a two-dimensional domain with a 512^2 mesh points. A two-step projection method [14] on a staggered arrangement grid was used for the pressure-velocity coupling. The piecewise linear interface reconstruction (PLIC) method [34] was used for the advection term of the VoF transport equation. The authors neglected the gas-phase dynamics, since the water density is three orders of magnitude greater than the air density. The numerical formulation was capable of predicting well the penetration depth, the coherent structures related to the water drop impacting the water pool and the bubble entrainment in the water-phase after the water drop impact. Apparently, the absence of the gas-phase dynamics in the simulations did not imply in any misrepresentation of the physics involved.

Hernández et al. [17] used the PLIC method to discretize the advection term of VoF equation in combination with a face-matched flux polyhedron advection (FMFPA-3D) method in order to substantially reduce the over/under lapping of flux polyhedron. This methodology was applied in a staggered arrangement grid where the pressure-velocity coupling is achieved using projection step. Unlike Morton et al. [23], Hernández et al. [17] considered the gas-dynamics in the momentum equation and the simulations were performed considering a three dimension domain. Owing to the symmetry of the problem, only a quarter of the domain was considered on a mesh with $140 \times 70 \times 70$ cells. Quantitatively and qualitatively speaking, very good agreement was obtained between numerical and experimental results with respect to the flow topology. In these two works, the splash problem was numerically evaluated by a geometric advection discretization of the VoF equation.

Despite the quality of the numerical results, such approach incurs substantial CPU time because of the several geometric operations involved. This is a non-negligible drawback when complex geometries are involved, which may require unstructured, topologically complex grids and when many droplets must be simulated. This scenario is not uncommon: liquid films that form in combustion chambers, for instance, are the result of continuous droplet splash. The occurrence as well as the thickness and velocity of the film strongly depend on the momentum and mass of the impacting droplets, so that a single droplet simulation would not be enough if these properties have to be calculated.

In view of this shortcoming, algebraic discretization methods for the VoF equation require considerably lower computational costs and are suitable for the representation of interfacial problems for average and instantaneous results [2,3,35]. One of the most common and reliable algebraic discretization method for the advection term of the VoF equation is the compressive interface capturing scheme for arbitrary meshes (CICSAM) method [33], which is based on the normalized variable diagram (NVD) [18]. According to Bussmann et al. [7], the density interpolation plays an important role on the interface advection for high density ratios (≥ 1000). In this regard, at least four different interpolation schemes for the density can be applied in an unstructured grid code: first order upwind scheme - FOU; second order upwind scheme - SOU; Central Differencing Scheme - CDS; and the volume-fraction weighted (VFW). Although all these interpolation schemes are widely used by the scientific community, so far no systematic research has been performed to numerically predict the influence of the density interpolation schemes of a water droplet splash. In this sense, the present work compares these four density interpolation schemes for two cases of a water drop splashing onto a deep water pool. In the following sections, modelings used in this work, numerical results and comparisons with experimental data are described.

2. Mathematical and physical modeling

Two-phase flows can be represented by the classical mass and momentum balance equations, respectively Eq. (3) and Eq. (4), for incompressible, laminar flows and immiscible fluids. Index notation and integral form are used to express mass and momentum equations as presented below.

$$\int_{sc} u_j \cdot n_j ds = 0, \tag{3}$$

$$\frac{\partial}{\partial t}\int_{cv}\rho u_i dv + \int_{sc}\rho u_i u_j \cdot n_j ds = -\int_{cs} p\delta_{ij}\cdot n_j ds + \int_{sc}\left[\mu\left(\frac{\partial u_i}{\partial x_j}+\frac{\partial u_j}{\partial x_i}\right)\right]\cdot n_j ds + \int_{cv}\rho g_i dv + f_{st}, \tag{4}$$

where: *cs* and *cv* represent, respectively, the control surface and the control volume; δ_{ij} is the Kronecker delta; u_i is the velocity vector; g_i is the gravity vector; μ is the dynamic viscosity of the fluid; ρ is the fluid density; and f_{st} is volumetric force related to the surface tension.

In the VoF method, two-phase flows are solved as one fluid with different physical properties. The volume fraction is defined as the ratio of the liquid volume and the total volume in a control volume $\left(\alpha = \frac{V_l}{V_l+V_g}\right)$. This scalar variable is bounded with $0 \le \alpha \le 1$ and indicates which phase is present in a specific point of the domain. In this work, the liquid phase is represented by $\alpha = 1$, whereas the gas phase by $\alpha = 0$. Density and viscosity in Eqs. (3) and (4) are weighted according to the volume fraction in the specific control volume, respectively Eq. (5) and Eq. (6), where the subscripts g and l indicate gas and liquid phases, respectively.

$$\rho = (1-\alpha)\rho_g + \alpha\rho_l, \tag{5}$$

$$\mu = (1-\alpha)\mu_g + \alpha\mu_l. \tag{6}$$

In this work, both phases are assumed incompressible, thus ρ_l and ρ_g are constant. The transport equation for the volume fraction (Eq. (7)) is obtained from the continuity equation for individual phases, using density relation with the volume fraction, Eq. (5),

$$\frac{\partial}{\partial t}\int_{cv}\alpha dv + \int_{sc}\alpha u_j \cdot n_j ds = 0. \tag{7}$$

Temporal changes in the phases location are evaluated through Eq. (7), so that the interface is placed in cells wherein $0 < \alpha < 1$. The interface is better described by a high numbers of cells in this vicinity, despite the different interpolation methods for the advection term in the scalar VoF equation.

The surface tension force is physically discontinuous, and defined only at the liquid-gas interface. However, from a numerical point of view, this effect should be modeled as continuous. The Continuum Surface Force model [5] was used to describe the term due to the surface tension force as a continuous force in the momentum equation. Thus, in the VoF method, the source term is related to the volume fraction gradient, the interface curvature and the surface tension coefficient of the pair of phases, Eq. (8),

$$f_{st} = \sigma\kappa\int_{sc}\alpha n_j ds. \tag{8}$$

The interface curvature can be obtained from the divergence of the unit vector to the interface [32], according to Eq. (9),

$$\kappa = -\nabla\cdot\left(\frac{\nabla\alpha}{|\nabla\alpha|}\right). \tag{9}$$

The complete geometry for the two cases consists in a cubic domain containing water and air in a quiescent condition. This condition is disturbed by the impact of an water drop onto the water pool. In Fig 2 the schematic for the splash cases is presented. Because of the symmetry of the problem, only a quarter of the domain was considered to reduce the computational cost. Furthermore, the water drop was released at the imminence to impact the water pool. The impact velocity was set in order to reproduce the one measured experimentally, and to consequently match the experimental Froude and Weber numbers. No-slip conditions were prescribed at the walls. All the dimensions of the Fig. 2 are scaled

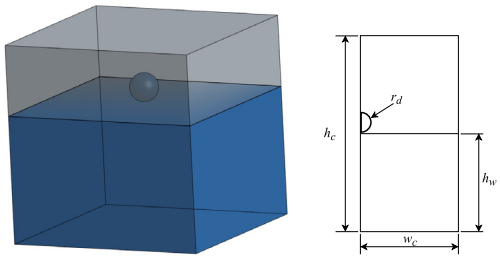

(a) Complete model. (b) A quarter of the domain.

Fig. 2. Schematic of the droplet in the imminence of impacting the water pool.

Table 1
Scaled dimensions of the splash cases.

dimensions	dimensions/d_d	
	case I	case II
h_c	7	9
h_w	4.5	4.5
w_c	3.5	3.5

using the water drop diameter ($d_d = 2.9$ mm). In Fig. 2(b), h_c is the height of the cavity, h_w is the height of the water pool, w_c is the width of the cavity considered (one quarter of the complete domain) and r_d is the water drop radius. In Table 1 the dimensions for the two cases studied in this work are shown.

3. Numerical approach

The finite volume method (FVM) [14], implemented on collocated, unstructured grids, was used to simulate all the splashing droplet cases. The code, named UNSCYFL3D, was developed in-house and can handle hybrid meshes and solve compressible and incompressible multiphase flows. For the pressure-velocity coupling, the SIMPLE method [14] was used. UNSCYFL3D has been extensively used for two-phase flows in a Euler-Lagrange framework and the respective numerical methods were properly validated in previous publications [8,9,11–13]. Other code features have already been reported in previous works and will not be repeated here. Thus, the next sections will discuss the details specifically related to the VoF model implemented and used in this work.

3.1. VoF model implementation

For the discretization of the VoF equation, Eq. (7), the Euler explicit scheme was employed for the temporal derivative, as Eq. (10) reads:

$$\frac{\partial}{\partial t}\int_{cv}\alpha dv \approx \frac{\alpha_p^{n+1}-\alpha_p^n}{\Delta t}V_{cv}, \tag{10}$$

where n indicates the current time step, $n+1$ the new time step, subscript p refers to the value of the variable at the cell center and V_{cv} is the volume of the cell or control volume.

The advective term was discretized considering that the velocity at the volume faces is the velocity at the face centroids, Eq. (11), as conventionally assumed in second-order finite-volume methods:

$$\int_{sc}\alpha u_j \cdot n_j ds \approx \sum_{f=1}^{N}\alpha_f \vec{u}_f \cdot \vec{n} A_f, \tag{11}$$

where N is the number of faces of the cell, $\vec{n}$ is the unit vector normal to the cell face f, $\vec{u}_f$ is the velocity vector at the centroid of face f and A_f is the face area.

The volume fraction at the cell faces could naively be approximated by conventional interpolation schemes, such as upwind and TVD schemes. However, the use of these schemes produces an excessive amount of numerical diffusion, which smooths the interface and deteriorates the results. Thus, specific discretization schemes have been devised for the solution of this equation. In this work, the CICSAM scheme was chosen for its low computational cost and for being capable of capturing sharp interfaces [32]. The CICSAM method presented by Ubbink [32] is a blend between upwind differencing and a differencing scheme obtained from the upper bound of convection boundedness criteria (CBC), presented by Gaskell and Lau [15].

The implementation of CICSAM in UNSCYFL3D is slightly different from that described by Ubbink [32] for arbitrary meshes. A pseudo-code is presented in the Algorithm 1.

Algorithm 1 CICSAM scheme on arbitrary meshes.

$\alpha_U \leftarrow \alpha_D + \nabla\alpha_D \cdot (\vec{x}_A - \vec{x}_D)$
$\alpha_U \leftarrow \max(\alpha_U, 0)$
$\alpha_U \leftarrow \min(\alpha_U, 1)$
$\tilde{\alpha}_D \leftarrow \frac{\alpha_D - \alpha_U}{\alpha_A - \alpha_U + \epsilon}$
$\theta \leftarrow \arccos\left(\frac{\nabla\alpha_D \cdot (\vec{x}_A - \vec{x}_D)}{|\nabla\alpha_D + \epsilon| \cdot |\vec{x}_A - \vec{x}_D|}\right)$
$\gamma_f \leftarrow \min\left(\frac{1+\cos 2\theta}{2}, 1\right)$
if $\tilde{\alpha}_D < 0$ or $\tilde{\alpha}_D > 1$ **then**
  $\alpha_{CBC} \leftarrow \tilde{\alpha}_D$
  $\alpha_{UQ} \leftarrow \tilde{\alpha}_D$
else
  $\alpha_{CBC} \leftarrow \min\left(1, \frac{\tilde{\alpha}_D}{\mathrm{Co}}\right)$
  $\alpha_{UQ} \leftarrow \min\left(\alpha_{CBC}, 8\,\mathrm{Co}\,\tilde{\alpha}_D + (1 - \mathrm{Co})\frac{6\tilde{\alpha}_D + 3}{8}\right)$
end if
$\tilde{\alpha}_f \leftarrow \gamma_f \alpha_{CBC} + (1 - \gamma_f)\alpha_{UQ}$
$\alpha_f \leftarrow \alpha_U + (\alpha_A - \alpha_U)\tilde{\alpha}_f$

In the above pseudo-algorithm, the $\sim$ represents normalized variables and ϵ is a tiny number, in the order of zero machine, to avoid divisions by zero. Subscripts A and D represent the Acceptor and Donor cells, respectively, which can be found based on the sign of mass flow rate through the face between both cells. *Co* represents the cell Courant number:

$$\mathrm{Co} = \sum_{f=1}^{N} \max\left(\vec{u}_f \cdot \vec{n} A_f \frac{\Delta t}{V_{cv}}, 0\right), \tag{12}$$

For the evaluation of the gradients in the equations above, the Node-Averaged-Gauss (NAG) scheme was used, as proposed by Marióc et al. [22].

A point that has not received much attention in previous works is the interpolation scheme to be employed for the cell face densities in the momentum equations. Even though it may be intuitive to assume that formally second-order methods such as SOU and CDS might produce the best results, investigations carried out in this work have shown that these may not be true for two-phase flows. Thus, in the next section the results of four interpolation schemes for the density at faces, namely the first-order upwind (FOU), the second-order upwind (SOU), the second-order central differencing (CDS) and the volume-fraction weighted (VFW) schemes, are presented and compared with the experimental results. For clarification purposes, the formulae for these schemes are shown below, using Fig. 3 as a reference.

3.1.1. First-Order Upwind scheme - FOU
if $\vec{u}_f \cdot \vec{n} > 0$ **then**
  $\rho_f = \rho_L$
else
  $\rho_f = \rho_R$
end if

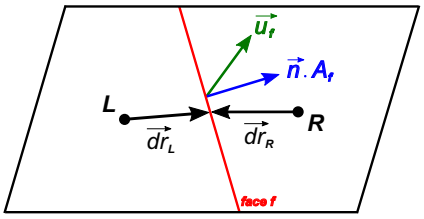

Fig. 3. Control volume discretization for the interpolation schemes.

3.1.2. Second-Order Upwind scheme - SOU
if $\vec{u}_f \cdot \vec{n} > 0$ **then**
  $\rho_f = \rho_L + \nabla\rho_L \cdot \vec{dr}_L$
else
  $\rho_f = \rho_R + \nabla\rho_R \cdot \vec{dr}_R$
end if

3.1.3. Central Differencing Scheme - CDS
$\rho_f = (\rho_L + \rho_R)/2$

3.1.4. Volume-Fraction Weighted - VFW
$\rho_f = (1 - \alpha_f)\rho_g + \alpha_f \rho_l$

Regarding the computational mesh, only hexahedra were used because of the simple geometry. Uniform grids with nearly two million elements were used for both cases.

A maximum Courant number of $\mathrm{Co} = 0.2$ led a time step of $\Delta t = 10^{-5}$ s which was used in both cases. The CPU time taken to solve the cases with this setup was approximately five days to reach about 0.03 s in physical time, using a serial simulation with an intel® i7-4790k processor with 8GB of RAM memory.

4. Results and discussions

In this section, the numerical results of the temporal development of the water droplet splash were analyzed, in the light of the respective theory and compared with the experimental results [23], for case *I* and case *II* (Table 1). Furthermore, four density interpolation schemes were investigated aiming to discover which density interpolation method is more suitable for the simulation of water splash problems.

In the real case, when the water drop is at the imminence to impact the water pool, it is expected that the downstream air pushes the free water surface. Sprittles [28], using kinetic theory in the gas film via Boltzmann equation, showed that the gas only influences the liquid phase through the pressure term in the normal direction of the interface, since usually $\mu_g/\mu_l << 1$, the tangential interaction is negligible.

In the numerical strategy, the water drop was released slightly above the water's free surface, with a little gap (≈ 0.2 mm) . However, this gap was found to be enough to capture the effect of the air pushing the free surface of the water pool, as shown in Fig. 4. In

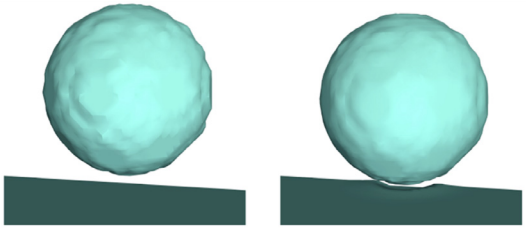

(a) First ime step. (b) Second ime step.

Fig. 4. The effect of the air pushing the free surface of the water pool.

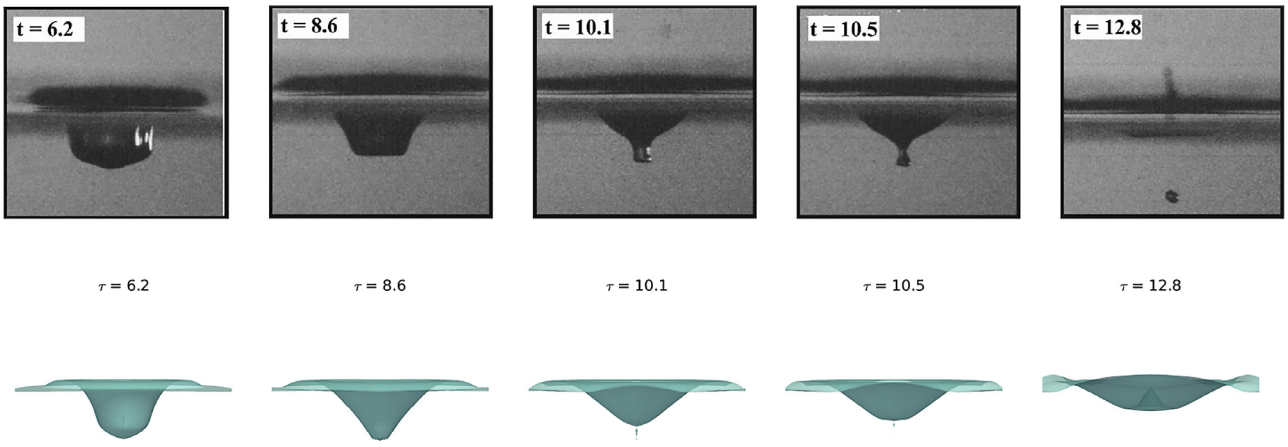

Fig. 5. Qualitative comparisons of the numerical splash topologies with images from Morton et al. [23] for the case I.

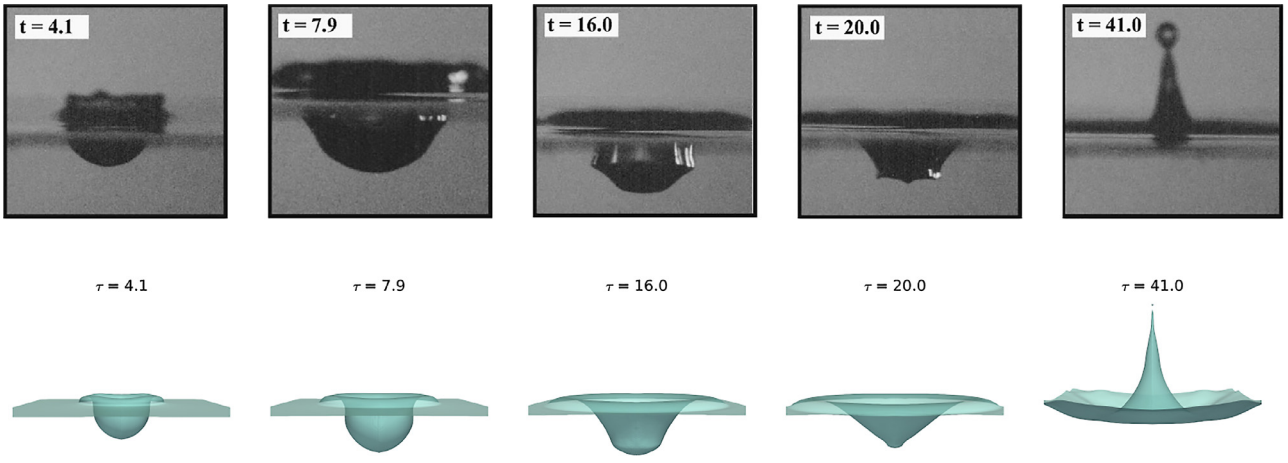

Fig. 6. Qualitative comparisons of the numerical splash topologies with images from Morton et al. [23] for the case II.

this figure an iso-volume of $\alpha = 0.5$ was used for case *I* using the CDS density interpolation method, although all the density interpolation methods were able to display the effect of the air pushing the water surface.

Temporal development of the water drop splash is an equally important qualitative result. The temporal evolution of the iso-volume of $\alpha = 0.5$, which was used to represent the interface, was compared to the experimental images of the temporal evolution of the water drop splash from Morton et al. [23], Figs. 5 and 6. The evolution comparisons were made considering the same dimensionless time, represented by the t and τ variables, respectively for the experimental and numerical data. The dimensionless time of each case was obtained multiplying the time by the ratio of the corresponding drop impact velocity and the drop diameter (U_l/d_d). In these simulations, the CDS density scheme was used.

At the beginning stages of the splash, the main features of the splash topologies were properly captured numerically for the two cases, even for different density interpolation schemes (not shown here). However, the reverse motion of the interface proved to be challenging for all density interpolation schemes, suggesting that for the reverse motion of the interface, algebraic discretization schemes of the advective term, such as CICSAM, are not the most suitable for capturing the splash topology properly. In this situation, a geometrical discretization scheme of the advective term has been shown to be more accurate [17,23].

In Figs. 7 and 8, topology differences using different density interpolation schemes are evidenced, respectively for case *I* and case *II*, at the final stage of the water splash. Clearly, the second order upwind (SOU) and first order upwind (FOU) schemes for density interpolation reduce the inertial effects, decreasing the jet peaks. In these schemes the interface density is mostly represented by the phase density upstream the interface motion direction. In the reverse motion (jet formation), the interface is highly influenced by the density of the liquid phase, reducing the normal pressure gradient in the interface which in turn reduces the height of the jet peak. Differently of the FOU and SOU, in the CDS and VFW schemes, the density interface is represented by the values of the adjacent cells (not only the cells in one direction), providing more realistic pressure gradient, closer to the qualitative experimental results. However, the interface reached the top wall of the numerical domain, exceeding the maximum height of the generated experimental jet. These differences in the maximum height may be related to the unbalance of the inertial and the surface tension forces. Since the surface tension force is calculated through the volume fraction gradients, Eqs. (8) and (9), and algebraic discretization schemes for the VoF method may not have high accuracy, the curvature was not rightly evaluated. An underestimation of the numerical surface tension force can be inferred, because the numerical height jet for the CDS and VFW density interpolation schemes exceed the experimental height jet and there was not droplet detachment. In fact, the inaccuracy on the surface tension force calculation does not prevent the comparison between the density interpolation schemes.

The depth of the crater created by the impact of the water drop on the pool surface was analyzed over time. Numerically, the depth created by the water drop impact was obtained by the distance

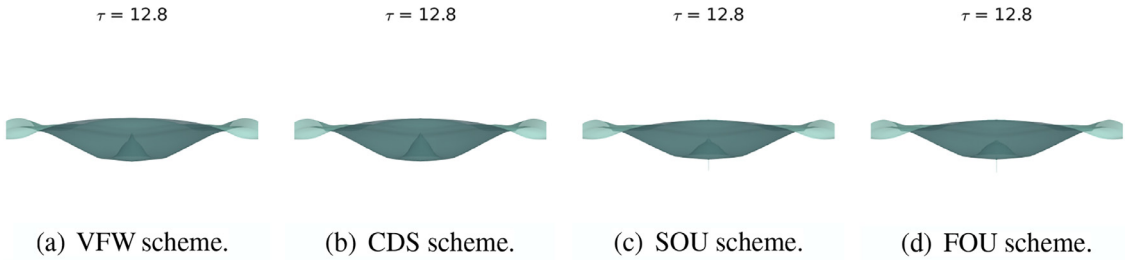

Fig. 7. Differences on the splash topology for the four density interpolation schemes for $\tau = 12.8$ in case *I*.

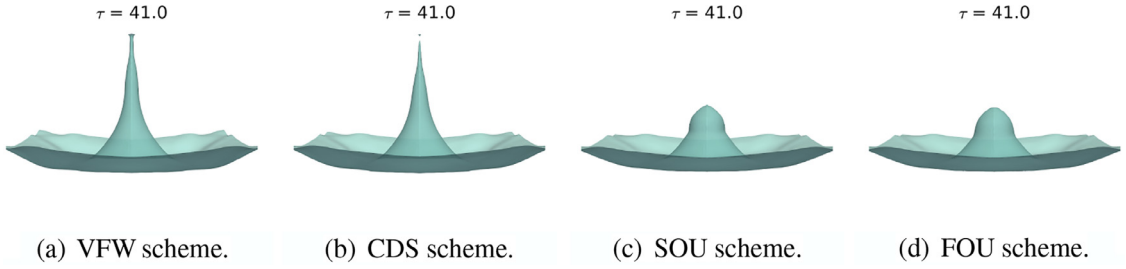

Fig. 8. Differences on the splash topology for the four density interpolation schemes for $\tau = 41.0$ in case *II*.

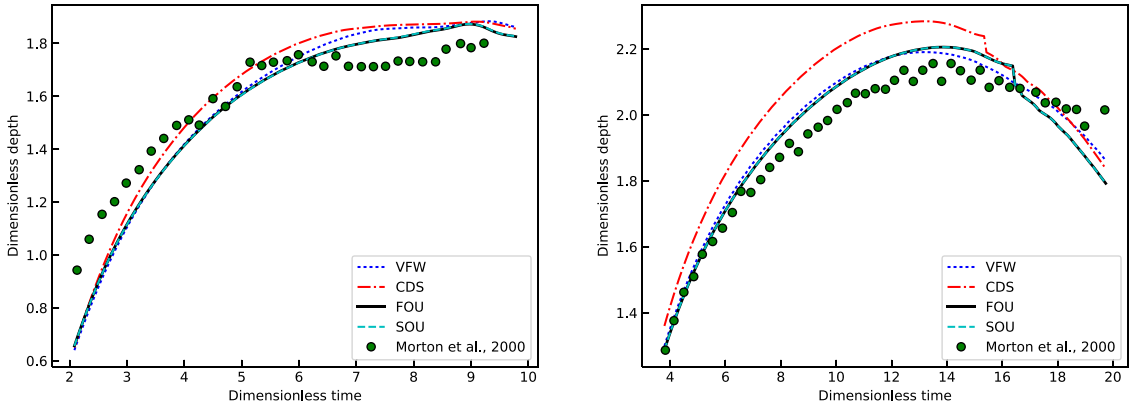

Fig. 9. Quantitative comparison of the dimensionless depth of the water splash cases.

from the free water pool surface before the water drop impact, to the interface on the line that intercepts the symmetry planes. The interface was considered to be at $\alpha = 0.5$. Numerical and experimental results of the splash depth were compared using the dimensionless depth (depth divided by the water drop) and time for the two studied cases, Fig. 9. All the density interpolation schemes have shown reasonable accuracy to predict the depth of the splash in the two cases, with a maximum difference of about 12%. No significant differences were found for the FOU and SOU density interpolation schemes, whereas the greater deviations from the experimental data were obtained for the CDS scheme, mainly for the case *II*, Fig. 9(b). Considering the temporal depth development, the particular selection of the best density interpolation scheme could not be made at this point.

Similarly to the crater depth, the resulting jet from the splash cases was analyzed over time. As mentioned before about the qualitative results, the reverse motion of the interface was not well predicted through the investigated methodology, Fig. 10. The FOU and SOU density interpolation schemes presented some differences between them, mainly for the case *II*, Fig. 10(b), but not significant compared to the experimental deviation. The CDS and VFW density interpolation schemes better match experimental data. Despite the differences in the dimensionless jet height in case *I*, about 50%, the VFW scheme presented the best agreement with the experimental data among the those investigated in this work.

5. Final remarks

Numerical simulations of droplet splash using high fidelity methodologies, such as geometric VoF schemes, might be impractical for cases involving many droplets, for example sprays and liquid films. Thus, in this work a computationally cheaper scheme was evaluated and compared to experimental results. In general, the main findings can be summarized as follows:

- The VoF/CICSAM method was able to predict reasonably the main features of the water splash, considering the usual difficulty found in simulating high density ratio ($\sim$1000) problems.

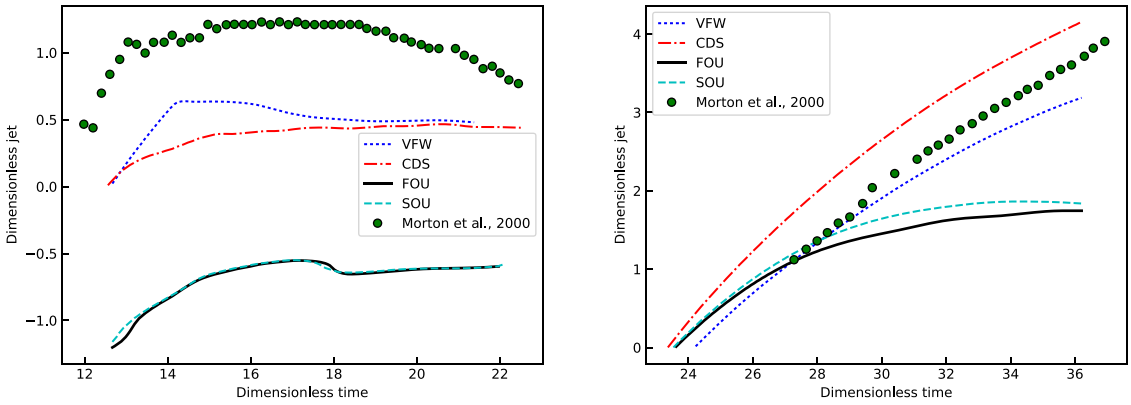

(a) Case *I*. (b) Case *II*.

Fig. 10. Quantitative comparison of the dimensionless jet height of the water splash cases.

- The results for the initial stages of the splash, i.e. up to the crater lowest valley, were satisfactory, including all density interpolation schemes tested;
- The accuracy of the CICSAM advective scheme deteriorates as the interface dynamics evolves from the crater valley to the ascending jet peak, irrespective of the density interpolation scheme. The VFW density interpolation scheme better matched the experimental results;
- To the best of the authors knowledge, this was the first work in which the density interpolation schemes for algebraic schemes of VoF method were assessed quantitatively in a physical problem. Despite the differences in jet height as compared with the experiment, the present model can be used for preliminary, fast estimates, or employed in real-scale simulations if the outcome of many droplets splash is to be calculated, for example in liquid film formation problem.

Acknowledgments

The authors acknowledge the support given by CNPq, CAPES and FAPEMIG to this research.

References

[1] C. Aalburg, B. Van Leer, G.M. Faeth, K.a. Sallam, Properties of nonturbulent round liquid jets in uniform gaseous cross flows, Atom. Sprays 15 (3) (2005) 271–294, doi:10.1615/AtomizSpr.v15.i3.20.
[2] M. Arienti, M. C. Soteriou, Dynamics of pulsed jet in crossflow(2007) 1–12.
[3] M. Arienti, L. Wang, M. Corn, X. Li, M.C. Soteriou, T.a. Shedd, M. Herrmann, Modeling wall film formation and breakup using an integrated interface-tracking/discrete-phase approach, J. Eng. Gas Turbines Power 133 (3) (2011) 031501, doi:10.1115/1.4002019.
[4] J. Becker, C. Hassa, Breakup and atomization of a kerosene jet in crossflow at elevated pressure, 2002. 10.1615/AtomizSpr.v12.i123.30
[5] J.U. Brackbill, D.B. Kothe, C. Zemach, A continuum method for modeling surface tension, J. Comput. Phys. 100 (2) (1992) 335–354, doi:10.1016/0021-9991(92)90240-Y.
[6] L. Bravo, C.-b. Kweon, A review on liquid spray models for diesel engine computational analysis, Army Res. Lab. (2014). May
[7] M. Bussmann, D.B. Kothe, J.M. Sicilian, Modeling high density ratio incompressible interfacial flows, ASME Fluids Eng. Div. Summer Meeting (2002) 707–713, doi:10.1115/FEDSM2002-31125.
[8] F.J. De Souza, R. De Vasconcelos Salvo, D.A. De Moro Martins, Large Eddy Simulation of the gas-particle flow in cyclone separators, Sep. Purif. Technol. 94 (2012) 61–70, doi:10.1016/j.seppur.2012.04.006.
[9] F.J. De Souza, A.L. Silva, J. Utzig, Four-way coupled simulations of the gas-particle flow in a diffuser, Powder Technol. 253 (2014) 496–508, doi:10.1016/j.powtec.2013.12.021.
[10] F. Denner, B.G.M. van Wachem, Fully-coupled balanced-force VOF framework for arbitrary meshes with least-squares curvature evaluation from volume fractions, Numer. Heat Transfer Part B 65 (3) (2014) 218–255, doi:10.1080/10407790.2013.849996.
[11] V.F. dos Santos, F.J. de Souza, C.A.R. Duarte, Reducing bend erosion with a twisted tape insert, Powder Technol. 301 (Supplement C) (2016) 889–910, doi:10.1016/j.powtec.2016.07.020.
[12] C.A.R. Duarte, F.J. de Souza, Innovative pipe wall design to mitigate elbow erosion: a cfd analysis, Wear 380-381 (Supplement C) (2017) 176–190, doi:10.1016/j.wear.2017.03.015.
[13] C.A.R. Duarte, F.J. de Souza, V.F. dos Santos, Numerical investigation of mass loading effects on elbow erosion, Powder Technol. 283 (2015) 593–606, doi:10.1016/j.powtec.2015.06.021.
[14] J. Ferziger, M. Perić, Computational Methods for Fluid Dynamics, 3rd, Springer-Verlag, Berlin Heidelberg, 2002.
[15] P.H. Gaskell, A.K.C. Lau, Curvature-compensated convective transport: SMART, anew boundedness- preserving transport algorithm, Int. J. Numer. Methods Fluids 8 (1988) 617–641, doi:10.1002/fld.1650080602.
[16] B.R. Halls, T.J. Heindel, A.L. Kastengren, T.R. Meyer, Evaluation of X-ray sources for quantitative two- and three-dimensional imaging of liquid mass distribution in atomizing sprays, Int. J. Multiphase Flow 59 (2014) 113–120, doi:10.1016/j.ijmultiphaseflow.2013.10.017.
[17] J. Hernández, J. López, P. Gómez, C. Zanzi, F. Faura, A new volume of fluid method in three dimensions-Part I: multidimensional advection method with face-matched flux polyhedra, Int. J. Numer. Methods Fluids 58 (8) (2008) 897–921, doi:10.1002/fld.1776.
[18] B.P. Leonard, The ULTIMATE conservative difference scheme applied to unsteady one-dimensional advection, Comput. Methods Appl. Mech.Eng. 88 (1991) 17–74.
[19] L.K.B. Li, S.I. Green, M.H. Davy, D.T. Eadie, Viscoelastic air-blast sprays in a cross-flow. Part 1: penetration and dispersion, Atom. Sprays 20 (8) (2010) 697–720.
[20] L.K.B. Li, S.I. Green, M.H. Davy, D.T. Eadie, Viscoelastic air-blast sprays in a cross-flow . Part 2 : droplet velocities, Atom. Sprays 20 (8) (2010) 721–735.
[21] Y. Ling, S. Zaleski, Multi-scale simulation of primary breakup in gas-assisted atomization, in: 53rd AIAA Aerospace Sciences Meeting, 2015, pp. 1–18.
[22] T. Marióć, H. Marschall, D. Bothe, voFoam A geometrical Volume of Fluid algorithm on arbitrary unstructured meshes with local dynamic adaptive mesh refinement using OpenFOAM, arXiv preprint arXiv:1305.3417, (2013) available online (http://arxiv.org/abs/1305.3417) 30.
[23] D. Morton, M. Rudman, J.-L. Liow, An investigation of the flow regimes resulting from splashing drops, Phys. Fluids 12 (4) (2000) 747, doi:10.1063/1.870332.
[24] H.N. Oguz, A. Prosperetti, Bubble entrainment by the impact of drops on liquid surfaces liquid surfaces, J. Fluid Mech. 219 (1990) 143–179, doi:10.1017/S0022112090002890.
[25] H.C. Pumphrey, L.A. Crum, Acoustic Emissions Associated with Drop Impacts, Springer Netherlands, Dordrecht, pp. 463–483. 10.1007/978-94-009-3017-9_34
[26] W. Samenfink, A. Elsäßer, K. Dullenkopf, S. Wittig, Droplet interaction with shear-driven liquid films: analysis of deposition and secondary droplet characteristics, Int. J. Heat Fluid Flow 20 (5) (1999) 462–469, doi:10.1016/S0142-727X(99)00035-1.
[27] Y.S. Shim, G.M. Choi, D.J. Kim, Numerical and experimental study on hollow-cone fuel spray of highpressure swirl injector under high ambient pressure condition, J. Mech. Sci. Technol. 22 (2) (2008) 320–329, doi:10.1007/s12206-007-1044-3.
[28] J.E. Sprittles, Kinetic effects in dynamic wetting, Phys. Rev. Lett. 6 (2017).
[29] C. Stevenin, A. Vallet, S. Tomas, M. Amielh, F. Anselmet, Eulerian atomization modeling of a pressure-atomized spray for sprinkler irrigation, Int. J. Heat Fluid Flow 57 (2016) 142–149, doi:10.1016/j.ijheatfluidflow.2015.11.010.
[30] M. Sussman, P. Smereka, S. Osher, A level set approach for computing solutions to incompressible two-phase flow, 1994, doi:10.1006/jcph.1994.1155.
[31] G. Tryggvason, B. Bunner, A. Esmaeeli, D. Juric, N. Al-Rawahi, W. Tauber, J. Han, S. Nas, Y.-J. Jan, A front-tracking method for the computations of multiphase flow, J. Comput. Phys. 169 (2) (2001) 708–759, doi:10.1006/jcph.2001.6726.

[32] O. Ubbink, Numerical prediction of two fluid systems with sharp interfaces, Splash (1997) 69, doi:10.1145/1774088.1774119.
[33] O. Ubbink, R.I. Issa, A method for capturing sharp fluid interfaces on arbitrary meshes, J. Comput. Phys. 153 (1999) 26–50.
[34] D.L. Youngs, Time-dependent multi-material flow with large fluid distortion, Numer. Methods Fluid Dyn. (1982) 273–285.
[35] D. Zhang, C. Jiang, D. Liang, Z. Chen, Y. Yang, Y. Shi, A refined volume-of-fluid algorithm for capturing sharp fluid interfaces on arbitrary meshes, J. Comput. Phys. 274 (2014) 709–736, doi:10.1016/j.jcp.2014.06.043.